THE JOURNAL OF PHYSICAL CHEMISTRY B

Article

pubs.acs.org/JPCB

Folic Acid-Conjugated LaF_3:Yb,Tm@SiO_2 Nanoprobes for Targeting Dual-Modality Imaging of Upconversion Luminescence and X-ray Computed Tomography

Jiebing Ma,[⊥] Peng Huang,[⊥] Meng He, Liyuan Pan, Zhijun Zhou, Lili Feng, Guo Gao, and Daxiang Cui*

Key Laboratory for Thin Film and Microfabrication of Ministry of Education, Institute of Micro-Nano Science and Technology, Shanghai Jiao Tong University, Shanghai 200240, P. R. China

Supporting Information

ABSTRACT: Development of multimodal contrast agents for *in vivo* simultaneous multimodality imaging is an emerging interdiscipline that is paving the avenue toward the goal of personalized medicine. Herein, folic acid-conjugated silica-modified LaF_3:Yb,Tm upconversion nanoparticles (UCNPs@SiO_2-FA) with high La content in a single particle were strategically designed and prepared for simultaneously targeting dual-modality imaging of upconversion luminescence (UCL) and X-ray computed tomography (CT). LaF_3 UCNPs were synthesized by a novel oleic acid (OA)/ionic liquid (IL) two-phase system. Afterward, a folic acid molecule was covalently anchored on the surface of UCNPs with a silane coupling agent. The UCNPs@SiO_2-FA exhibits good stability, water dispersibility and solubility, low cytotoxicity, good biocompatibility, highly selective targeting, excellent X-ray attenuation, and UCL emission under excitation at 980 nm. *In vivo* UCL and CT images of mice show the UCNPs@SiO_2-FA can be used in targeting dual-modality imaging. These results suggest that the as-prepared nanoprobe is a good candidate with excellent imaging and targeting ability for targeting dual-modality imaging of UCL and CT.

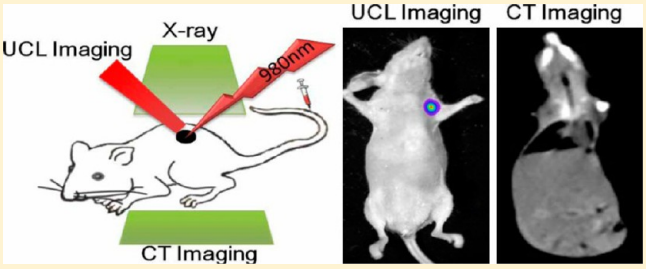

1. INTRODUCTION

Multimodality imaging refers to integrating the advantage of individual imaging modalities by fusing together information from several imaging techniques and, finally, arriving at a comprehensive imaging regimen.[1−8] It can compensate for the deficiencies of individual imaging modalities and satisfy the higher requirements on the efficiency and accuracy for diagnosis and research.[9] For example, fluorescence imaging with high sensitivity is often restricted due to its relatively poor resolution, whereas computed tomography (CT) and magnetic resonance imaging (MRI) with high spatial resolution are of insufficient sensitivity.[10−12] Thus, the combination of fluorescence imaging and CT/MRI could provide more complementary, effective, and accurate information about physical characteristics, anatomical structure, and physiological function.[13−16]

Lanthanide-based upconversion nanoparticles (UCNPs) have widely been used as building blocks in the construction of multimodal contrast agents for multimodality imaging because of their attractive merits, including narrow emission peaks, large antistokes shifts, excellent photostability, non-photoblinking, long lifetimes, and low toxicity.[17−22] Under continuous-wave (CW) excitation at 980 nm, UCNPs can convert low-energy light in the near-infrared (NIR) region into higher energy visible light through multiple photon absorption or energy transfer and produce unique upconversion luminescence (UCL) that promises a high signal-to-noise ratio (SNR) and deep light penetration for *in vivo* imaging.[14,23] So far, UCNPs exhibited great potential in applications such as NIR fluorescent imaging, MR imaging, and CT imaging of *in vivo* tumors, and targeted delivery of anticancer drugs in the near future.

Recently, we first reported lanthanide-doped $NaGdF_4$ upconversion nanocrystals are effective for dual-mode UCL imaging and CT imaging *in vivo*.[24] Since then, abundant research avalanched on the development of UCNPs as novel CT contrast agents.[9,14,25−28] To the best of knowledge, good CT contrast agents depend on the higher X-ray attenuation coefficient of their building blocks. For UCNPs as CT contrast agents, there are two approaches to improve the X-ray attenuation coefficient: (1) To increase the lanthanide elements content in a single particle. Gu et al. prepared the PEGylated Yb_2O_3:Er nanoparticles with high Yb content in a single particle suitable for both X-ray CT imaging and UCL imaging.[26] However, rare earth (RE) oxides are not the best luminescent rigid host matrix for various optically active Ln^{3+} ions in UCL. (2) To choose higher atomic number elements among RE elements for the preparation of UCNPs. Li et al. reported Lutetium (Lu)-UCNPs show strong X-ray absorption for CT imaging, because Lu has the largest atomic number among RE elements.[9,14,27] But the Lu content in a single $NaLuF_4$ particle is not the highest among all the RE fluorides (including REF_3

Received: September 12, 2012
Revised: November 5, 2012
Published: November 7, 2012

   dx.doi.org/10.1021/jp309059u | J. Phys. Chem. B 2012, 116, 14062−14070

Scheme 1. Schematic Representation of the Synthesis, Surface Functionalization, and Biological Applications of UCNPs@SiO_2-FA

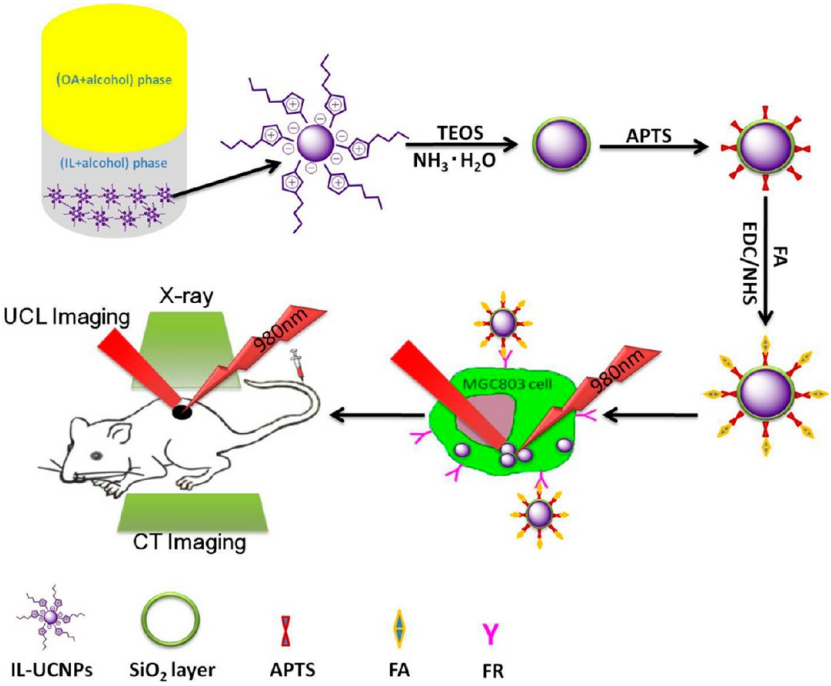

and $NaREF_4$). The RE contents in typical single $NaREF_4$ particles are as follows: $NaYF_4$ (Y = 47.3%), $NaGdF_4$ (Gd = 61.37%), $NaYbF_4$ (Yb = 63.6%), and $NaLuF_4$ (Lu = 63.87%). For all the REF_3 particles, although the lanthanum (La) is the smallest atomic number among RE elements, the La content in LaF_3 is 70.9%, much higher than other RE elements content in $NaREF_4$. Therefore, REF_3-based UCNPs can serve as excellent CT contrast agents and ideal building blocks for multimodal imaging agents.

In all the synthetic methods of UCNPs, the hydro(solvo)-thermal reaction system and thermal decomposition system are the well-developed methods to synthesize different structured UCNPs.[23,29−33] The obtained UCNPs in these two systems show high uniformity and monodispersity. However, it is worth noting that these two systems have intrinsic drawbacks.[34] For one thing, in the case of a hydro(solvo)thermal reaction system, handicaps still exist in crystal phase control while maintaining small sizes (<50 nm). For another thing, when it comes to a thermal decomposition system, these following defects are always mentioned: high temperatures (>300 °C), water-free conditions, an inert atmosphere, and the use of highly toxic organic precursors. Moreover, the obtained UCNPs are usually hydrophobic and need extra surface modification for further biological applications.[35] An ionic liquids (IL)-based synthesis system has emerged in recent years. The unique properties, including thermal and chemical stabilities, nonflammability, negligible vapor pressures, low melting points, and wide electrochemical windows, make IL highly suitable as a promising medium in synthetic strategies.[36−39] However, it should be noted that the IL-based synthesis system lacks capabilities in size control and crystal-phase manipulation while preparing UCNPs.[40] Recently, we combined the advantages of the three synthesis systems mentioned above and created an oleic acid (OA)/IL two-phase system to successfully prepare high-quality OA-capped UCNPs and water-soluble UCNPs with uniform morphologies and small sizes (<50 nm).[34] In the OA/IL two-phase system, water-soluble UCNPs can be obtained through the addition of alcohols (such as *n*-octanol and 1-hexanol) at the beginning of the reaction, which eliminate the cumbersome post-treatment procedures and facilitate their biological applications.[24] More importantly, the phases and sizes of UCNPs can be controlled by adding $BmimPF_6$ and alcohols (such as *n*-octanol) into the reaction system.[35]

In this present study, we selected gastric cancer MGC-803 cells as a research target, and strategically designed and prepared LaF_3-based UCNPs codoped with Yb^{3+} and Er^{3+}/Tm^{3+}/Ho^{3+} by an OA/IL two-phase system. Per surface functionalization of folic acid (FA), the FA-conjugated silica-modified LaF_3:Yb,Tm UCNPs were applied as multimodal imaging agents for simultaneously targeting dual-modality UCL imaging and CT imaging *in vivo*.

2. MATERIALS AND METHODS

2.1. Materials. Rare earth (RE) oxides in experiments, La_2O_3 (99.99%), Yb_2O_3 (99.99%), and Tm_2O_3 (99.99%) were purchased from Aladdin Chemistry. Oleic acid (OA), 1-hexanol, ethanol, ammonia, and tetraethylorthosilicate (TEOS) were obtained from Sinopharm Chemical Reagent. 1-Butyl-3-methylimidazolium hexafluorophosphate ($BmimPF_6$) was purchased from Shanghai Chengjie Chemical Co., Ltd. Folic acid (FA), 3-aminopropyltrimethoxysilane (APTS, >99%) carbodiimide (EDC), and *N*-hydroxysuccinimide (NHS) were obtained from J & K Chemical Limited. Deionized water (Millipore Milli-Q grade) was used throughout the series experiments. All the above chemicals were used without any further purification.

2.2. Synthesis of LaF_3: Yb, Tm Nanoparticles. RE-$(oleate)_3$ (RE = La, Yb, Tm) complexes were synthesized according to previously reported methods.[41,42] The as-synthesized $La(oleate)_3$ (0.78 mmoL), $Yb(oleate)_3$ (0.2 mmoL), and $Tm(oleate)_3$ (0.02 mmoL) were transferred into

dx.doi.org/10.1021/jp309059u | *J. Phys. Chem. B* 2012, 116, 14062−14070

a 50 mL Teflon-lined autoclave and then 15 mL of $BmimPF_6$ and 10 mL of 1-hexanol were added successively to form the two phase system. The autoclaves were then treated at 240 °C for 24 h. After cooling to room temperature (RT), the samples in the IL-phase were alternately washed with ethanol and deionized water several times. LaF_3: Yb, Tm UCNPs were recovered by centrifugation at 8500 rpm for 15 min. Subsequently, the samples were dried at 70 °C under vacuum overnight. LaF_3: Yb, Er and LaF_3: Yb, Ho UCNPs were synthesized by the same means.

2.3. Surface Modification of LaF_3: Yb, Tm UCNPs. Scheme 1 illustrates the synthesis, surface functionalization, and biological applications of UCNPs@SiO_2-FA. The as-prepared UCNPs (0.1 mmoL) were dispersed in ethanol (5 mL), and then ammonium hydroxide (0.1 mL, 28 wt %) was added, followed by ethanol (15 mL) containing TEOS (50 μL) under vigorous stirring. The entire system was vigorously stirred for 20 h at RT. UCNPs@SiO_2 were collected by centrifugation at 8500 rpm for 15 min and were washed three times with water and twice with ethanol. The obtained purified UCNPs@SiO_2 samples were redispersed in 30 mL of ethanol, and then 3 mL of APTS was added to form a mixture and allowed to react under refluxing at 80 °C for 3 h. The resultant was washed with deionized water for several times, and dried at 60 °C for 3 h in a vacuum oven to obtain the UCNPs@SiO_2-NH_2.

Covalent binding of FA to the UCNPs@SiO_2-NH_2 was conducted using a modification of the standard EDC-NHS reaction.[43,44] Carboxyl groups of FA (5 mg, 1.1×10^{-5} moL) were activated by an EDC/NHS solution (molar ratio of FA/EDC/NHS = 1:1:2.5) for 30 min. Afterward, 5 mg of UCNPs@SiO_2-NH_2 were added to form a mixed solution and allowed to react at RT for 12 h. The resultants were washed with deionized water and ethanol alternatively for removing unreacted chemicals by centrifugation. The obtained purified UCNPs@SiO_2-FA samples were redispersed into 10 mL of PBS for further characterization and applications.

2.4. Characterization. The sizes and morphologies of the as-prepared UCNPs were characterized by transmission electron microscopy (TEM) using a JEM-2010 microscope (JEOL, Japan) and high-resolution TEM (HR-TEM) on a JEM 2100F microscope (JEOL, Japan) with an acceleration voltage of 200 kV. X-ray diffraction (XRD) patterns were recorded on a Dmax-r C X-ray diffractometer (Rigaku, Japan) with Cu Kα radiation at 1.540 Å at a scanning rate of 6°/min in the 2θ range from 10° to 70°. Fourier transform infrared spectroscopy (FTIR) spectra were performed with an EQUINOX 55 spectrometer (Bruker, Germany). UV−vis spectra were measured with a Varian Cary50 UV−visible spectrophotometer equipped with a 10 mm quartz cell. The surface charge of samples was measured using a NICOMP 380ZLS ζ-potential/particle sizer. UCL spectra of LaF_3-based UCNPs codoped with Yb^{3+} and $Er^{3+}/Tm^{3+}/Ho^{3+}$ were characterized by using a Fluorolog-3 spectrofluorometer (Jobin Yvon, France) at RT.

2.5. Hounsfield Units of UCNPs@SiO_2-FA Measurement. The aqueous solution of UCNPs@SiO_2-FA with different concentrations in the range of 0−10 mg/mL was directly detected using a clinical CT (SIEMENS Spirit CT 31159, German). The attenuation values were obtained from the CT imaging software.

2.6. Cell Culture and Cytotoxicity Assay. Human gastric cancer MGC-803 cells (folate receptor (FR)-positive) and human normal gastric GES1 (FR-negative) cells were grown in RPMI-1640 medium with 10% fetal bovine serum (FBS) and 1% penicillin at 37 °C in a humidified 5% CO_2 atmosphere. MGC-803 cells and GES-1 cells (4×10^3 cells/well) were seeded in 96-well plates and incubated overnight. After being rinsed with PBS, the cells were incubated with varying concentrations of LaF_3: Yb, Tm UCNPs (0, 50, 100, 200, 400, 800 μg/mL) prepared above for 12 h at 37 °C in the dark under the same conditions. Cell viability was determined by methyl thiazolyl tetrazolium (MTT) assays. MTT (20 μL, 5 mg/mL) was added to each well, and then the plate was incubated for another 4 h. The medium was removed, and the formazan crystals formed were dissolved in 150 μL of dimethyl sulfoxide (DMSO). The absorbance at 570 nm for each well was recorded on the Thermo multiskan MK3 ELISA plate reader.

2.7. *In Vitro* Targeting Cell Ability of UCNPs@SiO_2-FA. About the targeting cell ability of UCNPs@SiO_2-FA, we evaluated the cellular selective uptake of UCNPs@SiO_2-FA with MGC-803 cells in RPMI-1640 medium without FA,[45] which were carried out contrasted to three other groups: (a) MGC-803 cells were treated with UCNPs@SiO_2-NH_2 in RPMI-1640 medium without FA; (b) MGC-803 cells were treated with UCNPs@SiO_2-FA in RPMI-1640 medium with FA; (c) GES-1 cells were treated with UCNPs@SiO_2-FA in RPMI-1640 medium without FA. MGC-803 and GES-1 cells were cultured on 20 mm glass coverslips in 6-well plates (2.5×10^5 cells/well) and preincubated for 24 h. After being rinsed with PBS (pH 7.4), the cells were incubated with 200 μg/mL of different samples for another 1 h. The glass coverslips were carefully rinsed with PBS three times, and cells were fixed using 4% paraformaldehyde solution for 15 min at RT. After being rinsed with PBS twice, the glass coverslips were transferred onto glass slides which already dropped 30% glycerol. Confocal imaging was performed using a modified Leica laser scanning confocal microscope, with a CW NIR laser at λ_{ex} = 980 nm as an additional excitation source. The emissions were collected in the range of 400−800 nm.

2.8. *In Vivo* CT Imaging. Male nude mice weighing 20−22 g were purchased from Shanghai SLAC Laboratory Animal Co. Ltd. (Shanghai, China). All animal procedures were in agreement with institutional animal use and care regulations. Nude mice were anesthetized with 100 μL of 10% chloral hydrate. 100 μL of UCNPs@SiO_2-FA (10 mg/mL) in PBS was subcutaneously injected into the back of mice and was intramuscularly injected into the left hind leg of mice, respectively. CT scans were performed using the above CT system.

2.9. *In Vivo* Lymphatic Dual-Modality Imaging. For *in vivo* lymphatic dual-modality imaging, UCNPs@SiO_2-FA (100 μL, 10 mg/mL) were intradermal injected into the right paw of the mice. UCL and CT images were acquired 1 h after the injection. UCL images were recorded on a modified IVIS Lumina XR (Xenogen Corporation-Caliper, Alameda, CA, USA) using an external 0−5 W adjustable CW infrared laser (980 nm, Shanghai Connet Fiber Optics Co., China) as the excited source. CT scans were performed using the above CT system.

2.10. *In Vivo* Targeting Tumor Tissue Ability of UCNPs@SiO_2-FA. Four-week-old male nude mice were injected s.c. on the right rear flank area with 5×10^6 MGC-803 cancer cells in 100 μL of serum free RPMI-1640 medium. After xenografts reached about 5 mm in diameter, the animals were randomized into two groups of three animals per group including control group and administration group. After

systemic tail vein injection of 200 μL of UCNPs@SiO_2-FA (3 mg/mL) per mouse, UCL images were acquired 2 h after the injection.

2.11. Statistical Analysis. All data are expressed in this article as mean result ± SD. All figures shown in this article were obtained from three independent experiments with similar results. All analyses were performed using Origin 8.0 software.

3. RESULTS AND DISCUSSION

3.1. Synthesis and Characterization of UCNPs@SiO_2. On the basis of our previous works, the synthetic principle and protocol of UCNPs are mature.[34] At the beginning, the reaction system was made up of three layers: 1-hexanol, OA phase, and IL phase. The precursors RE(oleate)$_3$ (RE = La, Yb, Tm) were dissolved in the OA phase. The whole system formed a homogeneous solution at elevated temperatures and pressures because of the cosolubility of 1-hexanol in both OA phase and IL phase. Meanwhile, the inducing factor 1-hexanol served as a "bridge" which paved a way for RE(oleate)$_3$ (RE = La, Yb, Tm, Er, Ho) to transfer from OA phase to IL phase. Surrounded by $Bmim^+$ cations and PF_6^- anions in IL phase, F^- released from PF_6^- and RE^{3+} reacted under coordination and Coulombic interactions, van der Waals forces, chemical bonds, and hydrogen bonds finally yielded $Bmim^+$-capped water-soluble LaF_3 UCNPs. Figure S1 in the Supporting Information shows the reaction-finished OA/IL two-phase system.

The morphologies and elemental compositions of as-prepared UCNPs were characterized by TEM, HR-TEM, and energy-dispersive X-ray (EDX) analysis. Figure 1A and B show that LaF_3: Yb, Tm UCNPs in the OA phase have high uniformity and monodispersity with an average size of 6.56 ± 1.16 nm (Supporting Information, Figure S2a). As shown in Figure 1C and D, UCNPs in the IL-phase are quasi-spherical with an average size of 11.25 ± 1.89 nm (Supporting Information, Figure S2b). The inset in Figure 1D shows the corresponding HR-TEM image. It reveals that the as-prepared UCNPs are highly crystalline and show the lattice distance of 0.18 nm, which can be indexed as the *d* spacing of the (302) lattice plane of the hexagonal LaF_3 structure. Figure 1E and F show the TEM and HR-TEM images of silica-coated UCNPs. They indicate that every UCNP is coated by a silica layer with the thickness of ~3 nm (Figure 1F). The thickness of the silica layer can be tuned in the range of 2−20 nm by the changes of the added amount of TEOS. The diffraction rings of the selected area electron diffraction (SAED) pattern (see the inset in Figure 1F) could be ascribed to the (002), (111), (300), (302), (411), and (330) planes of the hexagonal LaF_3 UCNPs lattice. The EDX analysis confirmed the presence of La, F, Yb, Tm in as-prepared UCNPs (Supporting Information, Figure S3).

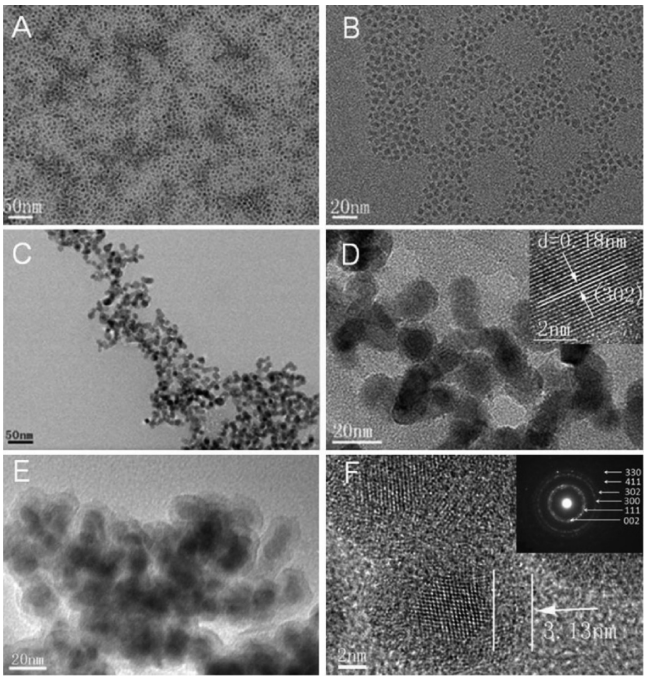

Figure 1. TEM images of (A, B) LaF_3: Yb, Tm UCNPs in the OA phase and (C, D) LaF_3: Yb, Tm UCNPs in the IL phase (inset: the corresponding HR-TEM image). (E, F) TEM images of UCNPs@SiO_2 (inset: the corresponding SAED pattern).

3.2. Characterization of UCNPs@SiO_2-FA. Figure 2A illustrates the XRD patterns of LaF_3: Yb, Tm UCNPs and UCNPs@SiO_2. For pure LaF_3: Yb, Tm UCNPs, all of the positions and intensities of the diffraction peaks are in good agreement with the JCPDS data (No. 32-0483), suggesting that the particles could be indexed to a pure hexagonal LaF_3 phase. After silica coating, there is a shoulder in the range of 20−25°, which can be ascribed to the amorphous silica. The result provides further evidence that the silica is successfully coated on the surface of UCNPs.

ζ-potentials of UCNPs, UCNPs@SiO_2, UCNPs@SiO_2-NH_2, and UCNPs@SiO_2-FA were recorded at pH 7.0 as shown in Figure 2B. The ζ-potential of pure UCNPs is 48.80 ± 1.81 mV, due to the existence of a lot of $Bmim^+$ on the surface of UCNPs. After silica coating, the ζ-potential of UCNPs@SiO_2 is −21.34 ± 4.90 mV, due to the existence of a lot of OH groups on the surface of UCNPs@SiO_2. The ζ-potential of UCNPs@SiO_2-NH_2 is 47.15 ± 8.20 mV, due to the existence of a lot of NH_2 groups on the surface of UCNPs@SiO_2-NH_2. After conjugation with FA, The ζ-potential of UCNPs@SiO_2-FA is −40.39 ± 3.22 mV, which indicates that the NH_2 groups on the surface of UCNPs@SiO_2-NH_2 are conjugated with FA. The results suggest that FA is successfully conjugated with UCNPs@SiO_2-NH_2.

To further confirm the successful conjugation between FA and UCNPs@SiO_2-NH_2, the UV−vis and FT-IR spectra of several typical samples were determined. Figure 2C shows the absorption spectra of UCNPs, UCNPs@SiO_2-NH_2, and UCNPs@SiO_2-FA. The spectra of UCNPs and UCNPs@SiO_2-NH_2 show no absorption peaks in the range of 200−500 nm. After conjugation with FA, the spectrum of UCNPs@SiO_2-FA displays a special peak at 285 nm, which is assigned to the $\pi \rightarrow \pi^*$ transition of the pterin ring of the FA molecule.[46] This result also proves that FA is successfully conjugated with UCNPs@SiO_2-NH_2. As shown in Figure 2D, there is an intensive peak at 1064 cm^{-1} in the spectra of UCNPs@SiO_2, UCNPs@SiO_2-NH_2, and UCNPs@SiO_2-FA, which is attributed to the characteristic absorption band of Si−O. This result suggests the presence of the silica layers on the surfaces of UCNPs. After conjugation with FA, the UCNPs@SiO_2-FA has new intensity absorption peaks at 562, 1519, and 2927 cm^{-1}, which are assigned to the bending vibration of methylene, the stretching vibration of the phenyl, and the characteristic alkyl (R-CH_2) stretch vibration, respectively. The above facts also prove that FA is successfully conjugated in UCNPs@SiO_2-NH_2.

dx.doi.org/10.1021/jp309059u | J. Phys. Chem. B 2012, 116, 14062−14070

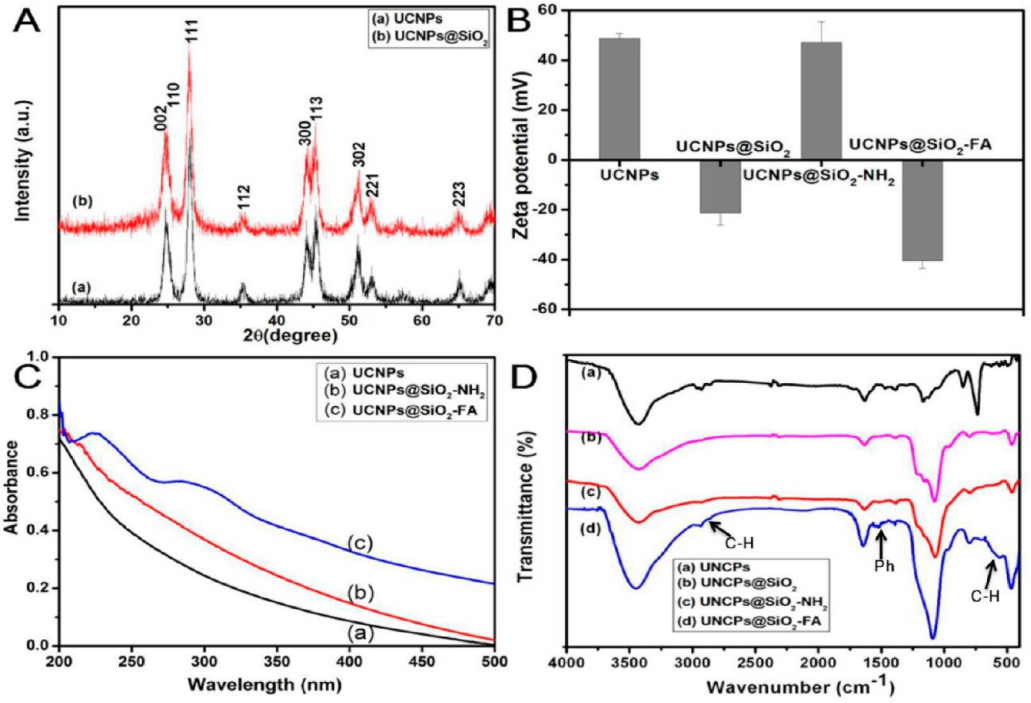

Figure 2. (A) XRD pattern of (a) LaF_3:Yb,Tm UCNPs and (b) UCNPs@SiO_2; (B) ζ-potential of UCNPs, UCNPs@SiO_2, UCNPs@SiO_2-NH_2, and UCNPs@SiO_2-FA; (C) UV−vis spectra of (a) UCNPs, (b) UCNPs@SiO_2-NH_2, and (c) UCNPs@SiO_2-FA; (D) FT-IR spectra of (a) UCNPs, (b) UCNPs@SiO_2, (c) UCNPs@SiO_2-NH_2, and (d) UCNPs@SiO_2-FA.

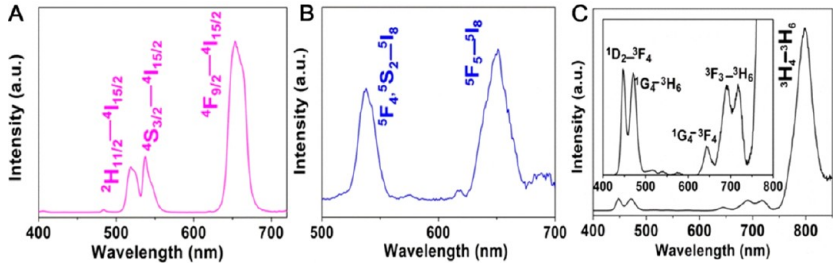

Figure 3. UCL spectra of (A) LaF_3: Yb, Er, (B) LaF_3: Yb, Ho, and (C) LaF_3: Yb, Tm UCNPs under excitation at a CW 980 nm laser.

3.3. UCL Properties of LaF_3 UCNPs Codoped with Yb^{3+} and $Er^{3+}/Tm^{3+}/Ho^{3+}$. Possessing distinguished UCL properties, UCNPs have their own advantages, which facilitates their further biological applications.[17,21] Figure 3 shows the UCL spectra of LaF_3 UCNPs codoped with Yb^{3+} and $Er^{3+}/Tm^{3+}/Ho^{3+}$. Figure 3A shows the UCL spectrum of LaF_3: Yb, Er UCNPs in the wavelength region 400−700 nm. The green emissions at 520 and 537 nm can be attributed to the $^2H_{11/2}-^4I_{15/2}$ and $^4S_{3/2}-^4I_{15/2}$ transitions, respectively. An intensive red emission centered at 653 nm was observed due to the transition from $^4F_{9/2}$ to $^4I_{15/2}$. Figure 3B shows the UCL spectra of Yb, Ho-codoped UCNPs under CW excitation at 980 nm. The emission band at around 540 nm was generated from the transition $^5F_4,^5S_2-^5I_8$, and the emission band at 650 nm can be assigned to the transition $^5F_5-^5I_8$. Under CW excitation at 980 nm, the Yb, Tm-codoped UCNPs displayed an intensive NIR emission band at around 800 nm, which could be assigned to the $^3H_4-^3H_6$ transition (Figure 3C). It is worth noting that emission at 800 nm is a perfect wavelength for *in vivo* imaging as a result of the deeper tissue penetration. Apart from the characteristic emission band at 800 nm, we could easily notice that other emission bands were located in the range 400−750 nm, corresponding to the $^1D_2-^3F_4$, $^1G_4-^3H_6$, $^1G_4-^3F_4$, and $^3F_3-^3H_6$ transitions, respectively. At the same time, Er^{3+}, Ho^{3+}, and Tm^{3+} ions doped hexagonal LaF_3 UCNPs have displayed high luminescent efficiency, especially the Tm^{3+} doped LaF_3 UCNPs with excellent NIR-to-NIR upconversion luminescence.[9,47] Therefore, the LaF_3: Yb, Tm UCNPs were investigated for further biomedical applications in this study.

3.4. Hounsfield Units of UCNPs@SiO_2-FA Measurement. UCNPs have potential as X-ray contrast agents because of their strong X-ray attenuation.[24] In this study, the Hounsfield units (HU) of UCNPs@SiO_2-FA were evaluated by a clinical CT. Figure 4A displays the CT images in the range of 0−10 mg/mL of UCNPs@SiO_2-FA. As the concentration of UCNPs@SiO_2-FA increased, the CT signal intensity continuously increased, resulting in brighter images. To further investigate the CT contrast effects, the attenuation values (HU) of UCNPs@SiO_2-FA at different concentrations were measured by CT software. As shown in Figure 4B, HU as a function of UCNPs@SiO_2-FA concentration display a well-correlated linear relationship (R^2 = 0.9988), described by the following typical equation: $Y = 17.28 - 0.533X$. These results

dx.doi.org/10.1021/jp309059u | J. Phys. Chem. B 2012, 116, 14062−14070

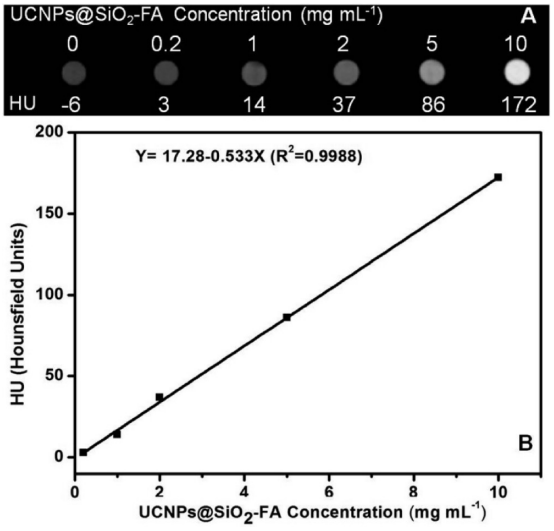

Figure 4. (A) *In vitro* CT images of UCNPs@SiO_2-FA suspended in PBS. The concentration (mg/mL) in each sample is provided at the top of the respective images. The corresponding HU value is provided at the bottom of the respective images. (B) CT attenuation (HU) plot of UCNPs@SiO_2-FA at various concentrations in the range from 0 to 10 mg/mL.

suggest that UCNPs@SiO_2-FA has a potential application as a positive X-ray/CT imaging contrast agent.

3.5. Cytotoxicity Assessment. Cytotoxicity assessment of as-prepared nanoprobes is essential to evaluate the potential for further biological applications of UCNPs@SiO_2-FA.[48,49] Figure 5 shows the cytotoxicity of UCNPs@SiO_2-FA to MGC-803

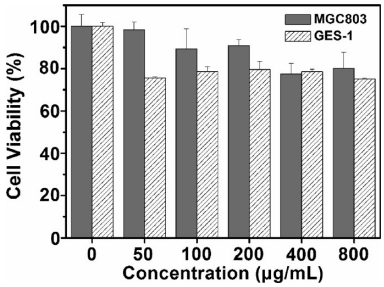

Figure 5. Cytotoxicity of UCNPs@SiO_2-FA to MGC-803 cells and GES-1 cells incubated with 0−800 μg/mL UCNPs@SiO_2-FA for 12 h at 37 °C in the dark. Cell toxicity was determined by MTT assay. Data represents mean ± SD (n = 5).

cells and GES-1 cells incubated with 0−800 μg/mL UCNPs@SiO_2-FA for 12 h at 37 °C in the dark. In the case of MGC-803 cells, no significant difference in cell viability is observed when the concentrations of UCNPs@SiO_2-FA ranged from 50 to 200 μg/mL. Even though the concentration goes up to as high as 800 μg/mL, cell viabilities are still greater than 80%. On the other hand, compared with their counterpart, GES-1 cells manifested lower cell viability against UCNPs@SiO_2-FA, mainly distribute in 75−79%, and did not decrease as the amount of nanoprobes increased; this phenomenon might be ascribed to the fact that the capability of antiadversity of normal cells is weaker than that of cancer cells. In light of the low cytotoxicity, UCNPs@SiO_2-FA could be an ideal fluorescent probe for further biological applications. These results fully show that UCNPs@SiO_2-FA possesses low cytotoxicity and excellent biocompatibility on MGC-803 cells and GES-1 cells within 0−800 μg/mL.

3.6. *In Vitro* Targeting Cell Ability of UCNPs@SiO_2-FA. To evaluate the *in vitro* targeting ability of UCNPs@SiO_2-FA, we performed confocal imaging with MGC-803 cells (FR-positive) incubated with UCNPs@SiO_2-FA, UCNPs@SiO_2-NH_2, UCNPs@SiO_2-FA and FA, and GES-1 cells (FR-negative) cultured with UCNPs@SiO_2-FA. Owing to the limitation of the Leica laser scanning confocal microscope, the upper limit of the collected emissive wavelength was confined to 800 nm. As shown in Figure 6A, MGC-803 cells cultured with UCNPs@SiO_2-FA display strong green UCL under CW excitation at 980 nm. The overlay of UCL and bright field images reveal that the UCL stems from the targeted UCNPs@SiO_2-FA on the surface of the cell membrane and intracellular UCNPs@SiO_2-FA (penetrated the cell membrane through receptor-mediated endocytosis). To support the receptor-mediated endocytosis of the nanoparticles, competition experiments between UCNPs@SiO_2-FA and FA were conducted (Figure 6C); no UCL signal is detected. Since all the conjugation sites are occupied by excess free FA, UCNPs@SiO_2-FA cannot specifically bind to FR. In Figure 6B (MGC-803 cells cultured with UCNPs@SiO_2-NH_2) and Figure 6D (GES-1 cells cultured with UCNPs@SiO_2-FA), no UCL signal is observed in both fluorescence and overlay images. To be noticed, only very weak background fluorescence is observed, suggesting that the as-prepared samples have a perfect signal-to-noise ratio. The above facts indicate that the FR on the surface of the membrane plays a vital role in the receptor-mediated endocytosis and UCNPs@SiO_2-FA has the capability of selectively targeting the MGC-803 cells.

3.7. *In Vivo* CT Imaging. To demonstrate the feasibility of UCNPs@SiO_2-FA for *in vivo* CT imaging, 2 mg/mL and 1 mg/mL of UCNPs@SiO_2-FA were subcutaneously injected into the back and the left rear flank area of mice, respectively. As shown in Figure 7, the subcutaneous injection site displayed an enhanced positive-contrast compared to that of other soft tissues, which is attributed to the strong X-ray attenuation induced by lanthanide elements. Meanwhile, the HU value of the injection site is more than the values of other tissues (such as bone, muscle), indicating that the synthesized UCNPs@SiO_2-FA is effective for CT imaging *in vivo*.

3.8. *In Vivo* Lymphatic Dual-Modality Imaging. To demonstrate the feasibility of UCNPs@SiO_2-FA for *in vivo* dual-modality imaging, UCNPs@SiO_2-FA (100 μL, 10 mg/mL per mouse) were intradermal injected into the right paw of the mice. As shown in Figure 8B, a clearly distinguished UCL signal is observed at the corresponding lymphatic node. Meanwhile, the lymphatic site displays an enhanced positive-contrast compared to other soft tissues (Figure 8 D), which is attributed to the fact that UCNPs@SiO_2-FA induces a strong X-ray attenuation. The results indicate that the synthesized UCNPs@SiO_2-FA nanoprobes are effective for dual-modality UCL and CT imaging *in vivo*.

3.9. *In Vivo* Targeting Tumor Tissue Ability of UCNPs@SiO_2-FA. According to the results of the *in vitro* targeting cell ability of UCNPs@SiO_2-FA, we perform *in vivo* imaging utilizing UCNPs@SiO_2-FA to specifically target gastric cancer. Nude mice loaded with gastric cancer MGC-803 cells were selected as the animal model. The tumors which were implanted and grown in mice to appropriate size (about 5 mm in diameter) were treated with intravenous injection of UCNPs@SiO_2-FA (200 μL 1 mg/mL per mouse). UCL

dx.doi.org/10.1021/jp309059u | J. Phys. Chem. B 2012, 116, 14062−14070

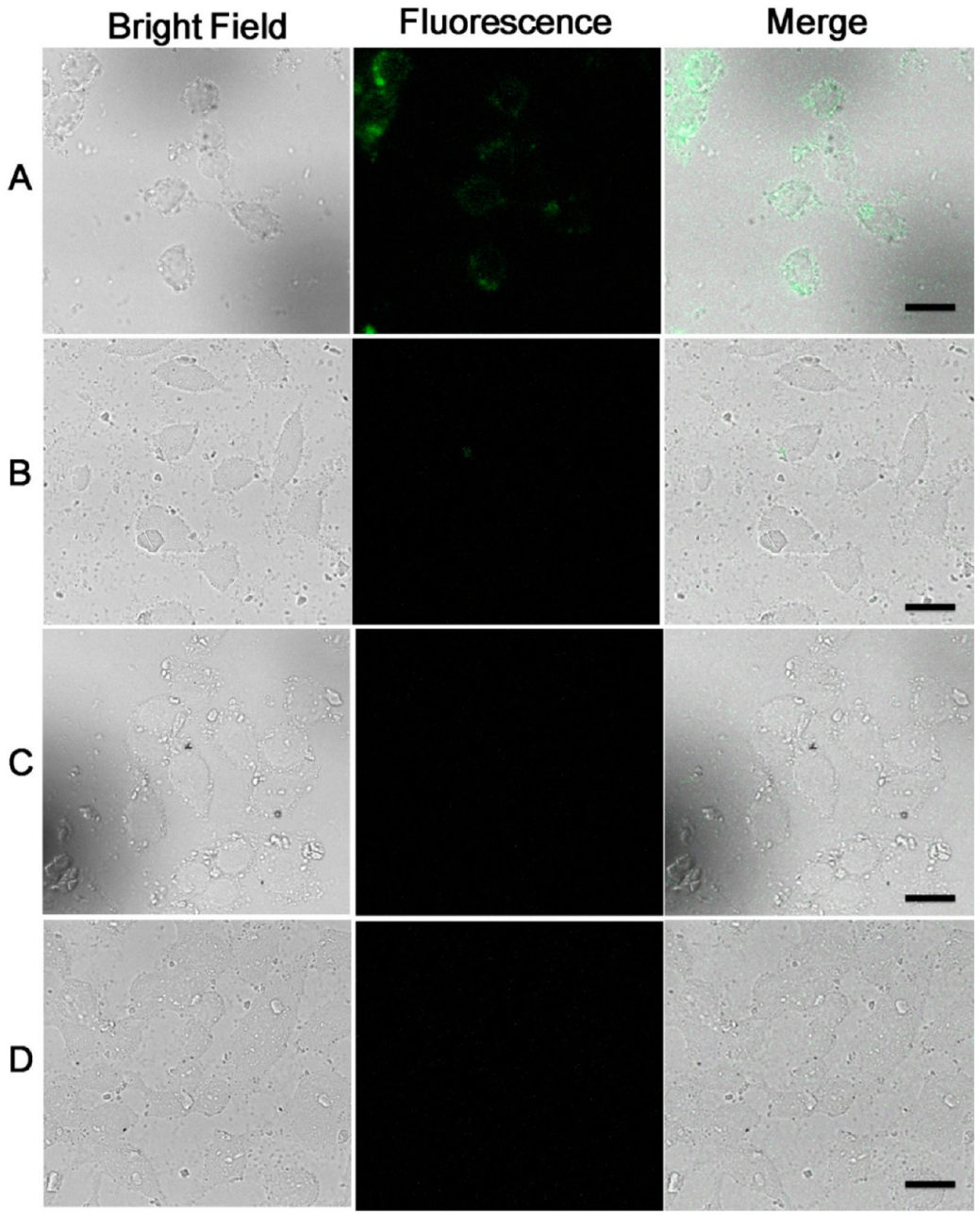

Figure 6. *In vitro* targeted imaging on MGC-803 cells and GES-1 cells. (A, B, C) MGC-803 cells were cultured with UCNPs@SiO_2-FA, UCNPs@SiO_2-NH_2, and UCNPs@SiO_2-FA + free FA, respectively. (D) GES-1 cells were cultured with UCNPs@SiO_2-FA. The emissions were collected in the range of 400−800 nm. The scale bar is 25 μm.

imaging was employed to monitor the targeting cancer tissue ability of UCNPs@SiO_2-FA during the whole blood circulation. Figure 9 shows real-time *in vivo* UCL images after intravenous injection of UCNPs@SiO_2-FA in nude mice at 2 h. The tumor tissue displays strong UCL signals in Figure 9A and C. Conversely, there are no obvious changes observed in the UCL images of the cancer tissues in the control group. These results are direct and clear evidence of gastric cancer cells targeted by the UCNPs@SiO_2-FA with a high specificity.

Biodistribution of UCNPs in nude mice was reported in previous reports.[50,51] It is widely accepted that liver and spleen are the two most UCNPs accumulation-oriented organs in nude mice, owing to the liver containing phagocytic cells, and they are the main organs for eliminating foreign particles. Besides, UCNPs also existed in bone, lung, heart, kidney, muscle, and blood, but compared with liver and spleen, their uptake was very low. In this study, FA modified UCNPs accumulated in tumor because of the targeting interaction between UCNPs@SiO_2-FA and the FR expressed on the surface of the gastric cancer cell membrane. Consequently, *in vivo* targeting dual-modality imaging using UCNPs is a feasible way to give us a new horizon for bioimaging application from the cellular scale to whole-body evaluation.

In order to develop the LaF_3-based UCNPs nanoprobes as multimodal contrast agents, a series of work should be undertaken: for example, to accurately control the size and morphology of prepared nanoprobes; to modify the surface of UCNPs using other specific biomarkers, such as peptides, antibodies, or aptamer at the same time, so that dual or multiple targeting purposes could be achieved; and to

dx.doi.org/10.1021/jp309059u | *J. Phys. Chem. B* 2012, 116, 14062−14070

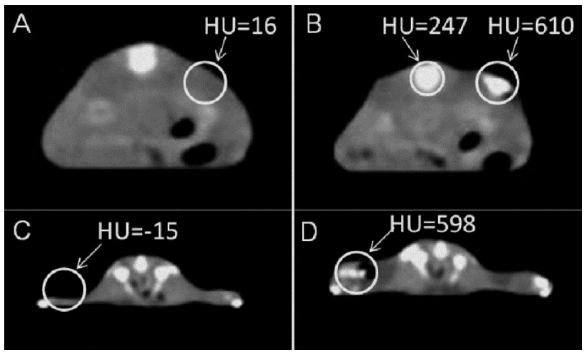

Figure 7. *In vivo* CT images of mice after injection with UCNPs@SiO_2-FA suspended in PBS: (A, B) the transverse image of the back, the HU value of the injection site is 610; (C, D) the transverse image of the buttock, the HU value of the injection site is 598.

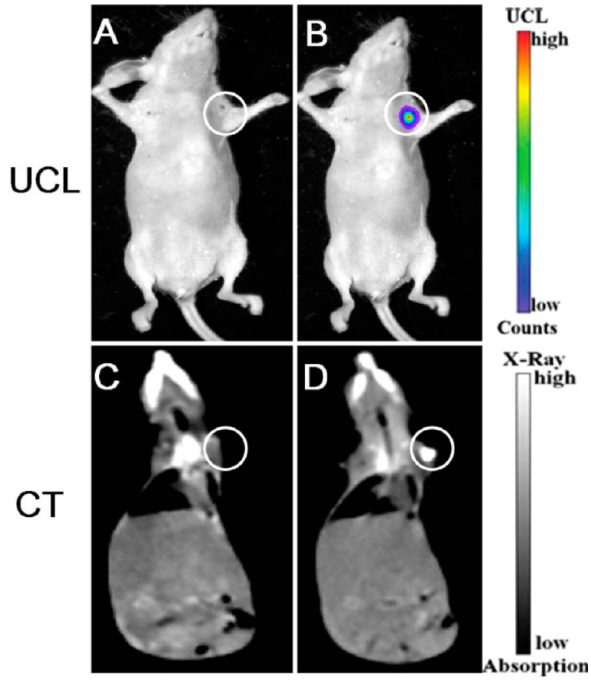

Figure 8. *In vivo* lymphatic node dual-modality imaging of UCL (A, B) and CT (C, D). (A, C) Before injection; (B, D) 1 h after injection. UCNPs@SiO_2-FA (100 μL, 10 mg/mL) were intradermal injected into the right paw of the mouse.

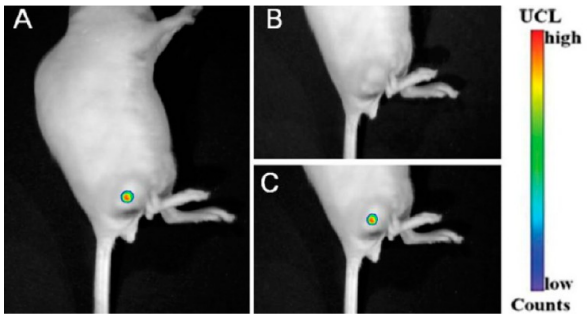

Figure 9. Real-time *in vivo* UCL images after intravenous injection of UCNPs@SiO_2-FA in nude mice at 2 h.

systemically investigate the toxicity, biocompatibility, pharmacokinetics, and biodistribution of the nanoprobes *in vivo*. Meanwhile, the development of multimodality imaging instruments is desired.

3. CONCLUSIONS

In summary, multimodal contrast agent based folic acid-conjugated silica-modified LaF_3:Yb,Tm upconversion nanoparticles (UCNPs@SiO_2-FA) with high La content in a single particle were strategically designed and developed. We have demonstrated that UCNPs@SiO_2-FA is a good candidate with excellent imaging and targeting ability for UCL imaging and CT imaging *in vivo*. The prepared UCNPs@SiO_2-FA exhibits good stability, water dispersibility, and solubility, low cytotoxicity, good biocompatibility, highly active targeting, excellent X-ray attenuation, and UCL emission under excitation at 980 nm. Our results show that the synthesized UCNPs@SiO_2-FA is effective for simultaneous targeting dual-modality imaging of UCL and CT, which could bring novel opportunities to the next generation of theranostic nanoprobes for simultaneous imaging diagnosis and therapy *in vivo*.

■ ASSOCIATED CONTENT

Ⓢ Supporting Information

Photograph of reaction-finished 1-hexanol-induced OA/IL two-phase system, histograms showing the size distribution of the LaF_3: Yb, Tm UCNPs in OA phase and IL phase, EDX analysis of the water-soluble LaF_3: Yb, Tm UCNPs in IL phase. This material is available free of charge via the Internet at http://pubs.acs.org.

■ AUTHOR INFORMATION

Corresponding Author

*E-mail: dxcui@sjtu.edu.cn.

Author Contributions

⊥Contributed equally to this paper.

Notes

The authors declare no competing financial interest.

■ ACKNOWLEDGMENTS

This work is supported by National Key Basic Research Program (973 Project) (No. 2010CB933901), National Natural Scientific Fund (No. 81225010, 51102258, 20803040, 81028009, 31170961), and New Century Excellent Talent of Ministry of Education of China (NCET-08-0350), 863key project (2007AA022004), and Important National Science & Technology Specific Projects (2009ZX10004-311).

■ REFERENCES

(1) Xie, J.; Liu, G.; Eden, H. S.; Ai, H.; Chen, X. *Acc. Chem. Res.* **2011**, *44*, 883−92.
(2) Xie, J.; Chen, K.; Huang, J.; Lee, S.; Wang, J.; Gao, J.; et al. *Biomaterials* **2010**, *31*, 3016−22.
(3) Cheng, L.; Yang, K.; Li, Y.; Chen, J.; Wang, C.; Shao, M.; et al. *Angew. Chem.* **2011**, *123*, 7523−8.
(4) Chen, F.; Huang, P.; Zhu, Y. J.; Wu, J.; Cui, D. X. *Biomaterials* **2012**, *33*, 6447−55.
(5) Chen, F.; Huang, P.; Zhu, Y. J.; Wu, J.; Zhang, C. L.; Cui, D. X. *Biomaterials* **2011**, *32*, 9031−9.
(6) Niu, G.; Chen, X. *Theranostics* **2012**, *2*, 413−23.
(7) Zhang, F.; Zhu, L.; Liu, G.; Hida, N.; Lu, G.; Eden, H. S.; et al. *Theranostics* **2011**, *1*, 302−9.
(8) Zhang, Y.; Yang, Y.; Cai, W. *Theranostics* **2011**, *1*, 135−48.
(9) Xia, A.; Chen, M.; Gao, Y.; Wu, D.; Feng, W.; Li, F. *Biomaterials* **2012**, *33*, 5394−405.

(10) Cai, W.; Chen, X. *J. Nucl. Med.* **2008**, *49*, 113S−28S.
(11) Townsend, D. *Phys. Med. Biol.* **2008**, *53*, R1−R39.
(12) Xu, H.; Cheng, L.; Wang, C.; Ma, X.; Li, Y.; Liu, Z. *Biomaterials* **2011**, *32*, 9364−73.
(13) Xie, J.; Lee, S.; Chen, X. *Adv. Drug Delivery Rev.* **2010**, *62*, 1064−79.
(14) Zhu, X.; Zhou, J.; Chen, M.; Shi, M.; Feng, W.; Li, F. *Biomaterials* **2012**, *33*, 4618−27.
(15) Cui, D.; Han, Y.; Li, Z.; Song, H.; Wang, K.; He, R; et al. *Nano Biomed. Eng.* **2009**, *1*, 61−74.
(16) Luo, T.; Huang, P.; Gao, G.; Shen, G.; Fu, S.; Cui, D; et al. *Opt. Express* **2011**, *19*, 17030−9.
(17) Zhou, J.; Liu, Z.; Li, F. *Chem. Soc. Rev.* **2012**, *41*, 1323−49.
(18) Wang, F.; Banerjee, D.; Liu, Y.; Chen, X.; Liu, X. *Analyst* **2010**, *135*, 1839−54.
(19) Wang, C.; Cheng, L.; Liu, Z. *Biomaterials* **2011**, *32*, 1110−20.
(20) Cheng, L.; Yang, K.; Zhang, S.; Shao, M.; Lee, S.; Liu, Z. *Nano Res.* **2010**, *3*, 722−32.
(21) Wang, M.; Mi, C. C.; Wang, W. X.; Liu, C. H.; Wu, Y. F.; Xu, Z. R.; et al. *ACS Nano* **2009**, *3*, 1580−6.
(22) Chen, G.; Ohulchanskyy, T. Y.; Kachynski, A.; Gren, H.; Prasad, P. N. *ACS Nano* **2011**, *5*, 4981−6.
(23) Wang, F.; Han, Y.; Lim, C. S.; Lu, Y.; Wang, J.; Xu, J; et al. *Nature* **2010**, *463*, 1061−5.
(24) He, M.; Huang, P.; Zhang, C.; Hu, H.; Bao, C.; Gao, G; et al. *Adv. Funct. Mater.* **2011**, *21*, 4470−7.
(25) Xing, H.; Bu, W.; Zhang, S.; Zheng, X.; Li, M.; Chen, F; et al. *Biomaterials* **2011**, *33*, 1079−89.
(26) Liu, Z.; Li, Z.; Liu, J.; Gu, S.; Yuan, Q.; Ren, J.; et al. *Biomaterials* **2012**, *33*, 6748−57.
(27) Zhou, J.; Zhu, X.; Chen, M.; Sun, Y.; Li, F. *Biomaterials* **2012**, *33*, 6201−10.
(28) Xing, H.; Bu, W.; Ren, Q.; Zheng, X.; Li, M.; Zhang, S.; et al. *Biomaterials* **2012**, *33*, 5384−93.
(29) Chen, Z.; Chen, H.; Hu, H.; Yu, M.; Li, F.; Zhang, Q.; et al. *J. Am. Chem. Soc.* **2008**, *130*, 3023−9.
(30) Wang, X.; Zhuang, J.; Peng, Q.; Li, Y. *Nature* **2005**, *437*, 121−4.
(31) Mai, H. X.; Zhang, Y. W.; Si, R.; Yan, Z. G.; Sun, L.; You, L. P.; et al. *J. Am. Chem. Soc.* **2006**, *128*, 6426−36.
(32) Boyer, J. C.; Vetrone, F.; Cuccia, L. A.; Capobianco, J. A. *J. Am. Chem. Soc.* **2006**, *128*, 7444−5.
(33) Yi, G. S.; Chow, G. M. *Chem. Mater.* **2007**, *19*, 341−3.
(34) He, M.; Huang, P.; Zhang, C.; Chen, F.; Wang, C.; Ma, J.; et al. *Chem. Commun.* **2011**, *47*, 9510−2.
(35) He, M.; Huang, P.; Zhang, C.; Ma, J.; He, R.; Cui, D. *Chem.—Eur. J.* **2012**, *18*, 5954−69.
(36) Hapiot, P.; Lagrost, C. Electrochemical reactivity in room-temperature ionic liquids. *Chem. Rev.* **2008**, *108*, 2238−64.
(37) Zhang, C.; Chen, J. *Chem. Commun.* **2010**, *46*, 592−4.
(38) Hu, H.; Yang, H.; Huang, P.; Cui, D.; Peng, Y.; Zhang, J.; et al. *Chem. Commun.* **2010**, *46*, 3866−8.
(39) Liu, X.; Zhao, J.; Sun, Y.; Song, K.; Yu, Y.; Du, C.; et al. *Chem. Commun.* **2009**, 6628−30.
(40) Li, C.; Lin, J. *J. Mater. Chem.* **2010**, *20*, 6831−47.
(41) Wei, Y.; Lu, F.; Zhang, X.; Chen, D. *Chem. Mater.* **2006**, *18*, 5733−7.
(42) Park, J.; An, K.; Hwang, Y.; Park, J. G.; Noh, H. J.; Kim, J. Y.; et al. *Nat. Mater.* **2004**, *3*, 891−5.
(43) Johnsson, B.; Löfås, S.; Lindquist, G. *Anal. Biochem.* **1991**, *198*, 268−77.
(44) Huang, P.; Li, Z.; Lin, J.; Yang, D.; Gao, G.; Xu, C.; et al. *Biomaterials* **2011**, *32*, 3447−58.
(45) Huang, P.; Xu, C.; Lin, J.; Wang, C.; Wang, X.; Zhang, C.; et al. *Theranostics* **2011**, *1*, 240−50.
(46) Huang, P.; Bao, L.; Zhang, C.; Lin, J.; Luo, T.; Yang, D.; et al. *Biomaterials* **2011**, *32*, 9796−809.
(47) Zhou, J. C.; Yang, Z. L.; Dong, W.; Tang, R. J.; Sun, L. D.; Yan, C. H. *Biomaterials* **2011**, *32*, 9059−67.
(48) Sun, Y.; Chen, Z.; Yang, X.; Huang, P.; Zhou, X.; Du, X. *Nanotechnology* **2009**, *20*, 135102.
(49) Chen, Z. L.; Sun, Y.; Huang, P.; Yang, X. X.; Zhou, X. P. *Nanoscale Res. Lett.* **2009**, *4*, 400−8.
(50) Zhou, J.; Yu, M.; Sun, Y.; Zhang, X.; Zhu, X.; Wu, Z.; et al. *Biomaterials* **2011**, *32*, 1148−56.
(51) Sun, Y.; Yu, M.; Liang, S.; Zhang, Y.; Li, C.; Mou, T.; et al. *Biomaterials* **2011**, *32*, 2999−3007.